Int. J. Electrochem. Sci., 8 **(2013)** 8669 - 8685

International Journal of
ELECTROCHEMICAL
SCIENCE
www.electrochemsci.org

Synthesis, Spectral and Quantum Chemical Calculations of Mononuclear Nickel(II), Copper(II) and Cadmium(II) Complexes of New Schiff–Base Ligand

Muneerah M. Al-Mogren[1] *and Abdel-Nasser M. A. Alaghaz*[2,3*]

[1]Department of Chemistry, Faculty of Science, King Saud University, Riyadh, Saudi Arabia P.O.Box 2455 riyadh 11451
[2]Department of Chemistry, Faculty of Science, Al–Azhar University, Nasr City, Cairo, Egypt
[3]Department of Chemistry, Faculty of Science, Jazan University, Jazan, Saudi Arabia

[*]E-mail: aalajhaz@hotmail.com, aalajhaz@yahoo.com

Received: 21 March 2013 / *Accepted:* 14 May 2013 / *Published:* 1 June 2013

The complexes of type $[Ni(L)_2(H_2O)_2]2H_2O$, $[Cu(L)_2(H_2O)_2]$, and $[Cd\text{-}(L)_2(H_2O)_2]H_2O$, where L = salicylidene–4–chlorophenyl–2–aminothiazole, have been synthesized by condensation of salicylaldehyde and 4–chlorophenyl–2–aminothiazole (2:1) in the presence of divalent metal salt in methanolic medium. The ligand and its metal complexes have been characterized with the help of elemental analysis, IR, MS, UV–Vis, ^1H and ^{13}C NMR, ESR, XRD, CV, thermal analysis, magnetic susceptibility and molar conductance measurements. From the modeling studies, the bond length, bond angle, core-core interaction, heat of formation, electronic energy, binding energy, HOMO, LUMO and dipole moment had been calculated to confirm the geometry of the ligand and their investigated complexes. The antimicrobial results indicate that the cadmium complex exhibit more activity than the nickel (II) and copper (II) complexes.

Keywords: Schiff base; Transition metal complexes; Spectra; Antimicrobial activity

1. INTRODUCTION

The condensation of primary amines with carbonyl compounds yields Schiff bases [1,2]. Schiff base with donors (N, O, S, etc) have structure similarities with neutral biological systems and due to presence of imine group are utilized in elucidating the mechanism of transformation of rasemination reaction in biological system [3–5]. Thiazole and its derivatives as ligands with potential sulphur and nitrogen bands are interesting and have gained special attention not only the structural chemistry of their multifunctional coordination modes but also of their importance in medicinal and pharmaceutical field. They show biological activities including antibacterial antifungal [6], antidiabetic [7], antitumor [8], antiproliferative [9], anticancer [10], herbicidal [11]. Schiff bases represent an important class of compounds because they are utilized as starting materials in the synthesis of industrial products [12].

Moreover, Schiff bases are regarded as privileged ligands [13]. Due to their capability to form complexes with different transition metals can act as catalysts for many different reactions [14, 15].

We were thus motivated to undertake a systematic study of preparation and characterization of transition metal complexes formed with salicylidene–4–chlorophenyl–2–aminothiazole (HL) and Ni(II), Cu (II) and Cd(II) ions.

2. EXPERIMENTAL

2.1. Synthesis of ligand (HL)

4–chlorophenyl–2–aminothiazole (5.22 g, 24.88 mmol) dissolved in methanol (10 mL) was added slowly with constant stirring to KOH in methanol. The solution was stirred for half an hour and then filtered. To the filtrate salicylaldehyde (3.03 g, 24.88 mmol) dissolved in MeOH (20 mL) was added drop wise with constant stirring. The resulting solution was evaporated under reduced pressure and kept at room temperature for 2 h. The dirty orange precipitate was washed with cold alcohol. The crystals were suction filtered washed with diethyl ether and dried in vacuum. The product was found to be TLC pure in 7:3 mixtures of methanol and chloroform (mobile phase). The melting points, colours, yields, stoichiometries, elemental analyses, and molar conductances of the ligand are given in Table 1.

2.1.1. Synthesis of the metal (II) complexes

The metal complexes of the Schiff base HL was prepared by the addition of hot solution (60 °C) of the appropriate metal chloride (0.001 mmol) in methanol (8 mL) to the hot solution (75 °C) of the Schiff base (0.629 g HL, 0.002 mmol) in methanol (25 mL). The resulting mixture was stirred under reflux for 2 h where upon the complexes precipitated. They were collected by filtration and purified by washing with methanol and dried under vacuum over anhydrous $CaCl_2$. The melting points, colours, yields, stoichiometries, elemental analyses, and molar conductances of the complexes are given in Table 1.

2.2. Materials

All chemicals used were of the analytical reagent grade (AR), and of highest purity available. They included salicylaldehyde (Sigma) and 4-chlorophenyl-2-aminothiazole (Sigma). $NiCl_2.6H_2O$ (BDH), $CuCl_2.2H_2O$ (Sigma), and $CdCl_2.2.5H_2O$ (Sigma) were used. Organic solvents used included absolute ethyl alcohol, diethyl ether, diethylamine, formaldehyde and dimethylformamide (DMF).

2.3. Physical measurements

All melting points were taken on a Stuart apparatus and are uncorrected. Elemental microanalyses of the solid chelates for C, H, N, S and Cl were performed at the Microanalytical Center, Cairo University. Metal contents were estimated on an AA-640-13 Shimadzu flame atomic absorption spectrophotometer in solution prepared by decomposing the respective complex in hot concentrated HNO_3. The molar conductance of solid chelates in DMF was measured using Sybron-Barnstead conductometer (Meter-PM.6, E = 3406). Their IR spectra were recorded on Perkin-Elmer FT-IR spectrophotometer in nujol mull and polyethylene pellets. The UV–visible absorption spectra were recorded using Jasco V-350 recording spectrophotometer at room temperature. The molar magnetic susceptibility was measured on powdered samples using the Faraday method. The diamagnetic corrections were made by Pascal’s constant and $Hg[Co(SCN)_4]$ was used as a calibrant. The mass spectra were recorded by the EI technique at 70 eV using MS-5988 GC–MS Hewlett–Packard instrument in the Microanalytical Center, Cairo University. The ^1H (300 MHz) and ^{13}C NMR (75 MHz) spectra were recorded using 300 MHz Varian–Oxford Mercury. The deuterated solvent used was dimethylsulphoxide (DMSO) and the spectra extended from 0 to 15 ppm. Electrochemical behavior of the metal complexes was investigated with CH Instruments, U.S.A (Model 1110A-Electrochemical analyzer, Version 4.01) in HPLC grade DMF containing n-Bu4NClO4 as the supporting electrolyte. The three-electrode system consisted of glassy carbon electrode (3 mm diameter) as a working electrode, a Ag/AgCl (3 M KCl) reference electrode and a platinum wire as auxiliary electrode was used. In order to provide a reproducible active surface and to improve the sensitivity and resolution of the voltammetric peaks, the glassy carbon electrode was polished to a mirror finish with 0.3 micron alumina on a smooth polishing cloth and then rinsed with methanol and double distilled water prior to each electrochemical measurements. The electrode cleaning procedure requires less than 3 min. All the solutions examined by electrochemical techniques were purged for 10 min with water-saturated nitrogen. All measurements were carried out at room temperature (24 °C).

3. COMPUTATIONAL METHODS

An attempt to gain a better insight on the molecular structure of the ligand and its complexes, geometry optimization and conformational analysis has been performed using MM+ force–field as implemented in hyperchem 8.03 [16]. The low lying obtained from MM+[17] was then optimized at PM3 using the Polak–Ribiere algorithm in RHF–SCF, set to terminate at an RMS gradient of 0.01 kcal mol^{-1}.

4. RESULTS AND DISCUSSION

4.1. The ligand

The characteristic IR spectral data for HL (Figure 1) compound are presented in the Table 2. The bands centered at about 3445 cm^{-1} are assigned to ν(O–H) in O–H……N intramolecular hydrogen–bonding fragment. Very strong bands centered at 1641 cm^{-1} are assigned to ν(C=N) stretching in HL ligand.

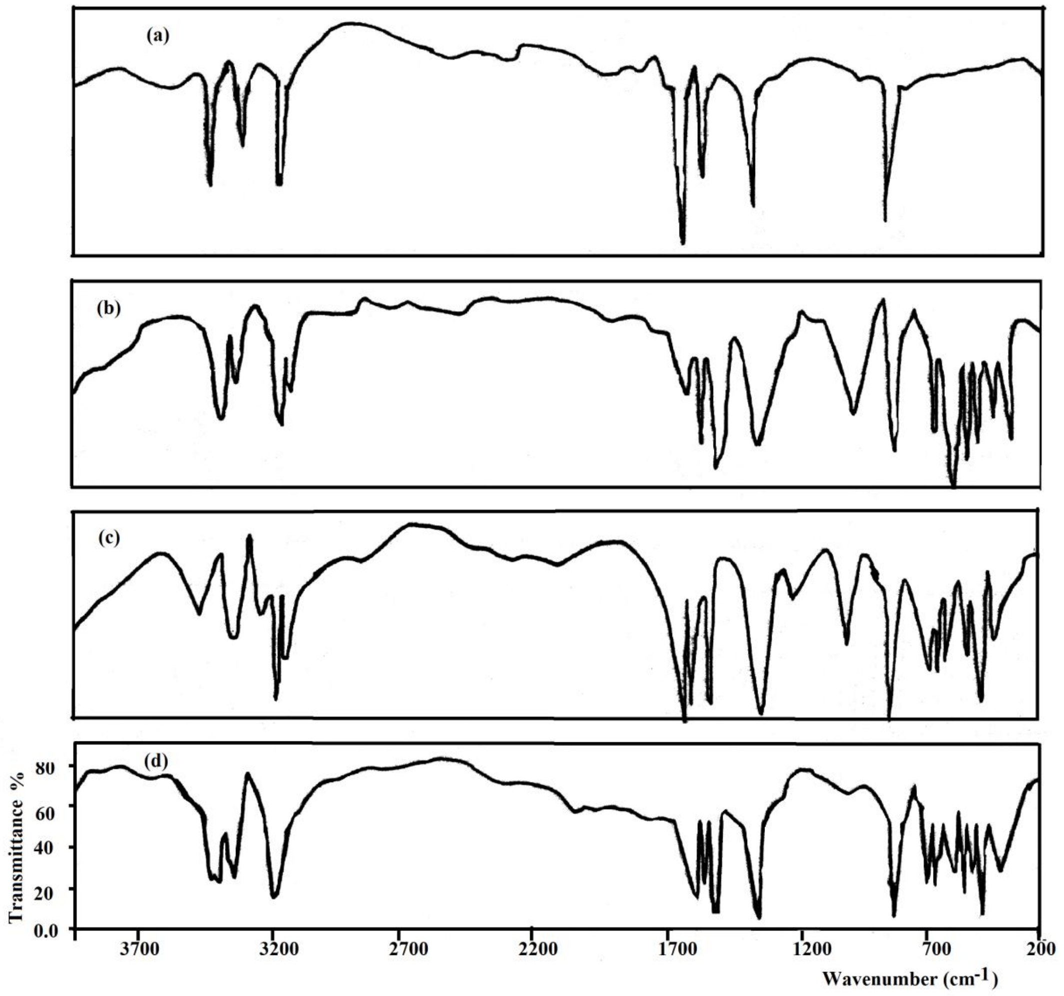

Figure 1. FT–IR spectra of: (a) HL ligand, (b) $[Ni(L)_2(H_2O)_2].2H_2O$, (c) $[Cu(L)_2(H_2O)_2]$ and (d) $[Cd(L)_2(H_2O)_2].H_2O$.

Table 1. Melting points, colours, yield and partial elemental analyses data of the ligand (HL) and its corresponding metal complexes

Compound no. M. F.	m.p. (°C)	Color [Yield (%)]	Elemental analyses % calculated (found)						$^a\Lambda_m$
			M	C	H	N	S	Cl	
HL	160-162	Orange [98]	--	61.05 (61.00)	3.52 (3.44)	8.90 (8.25)	10.19 (10.12)	11.26 (11.24)	2.45
(1)$[Ni(L)_2(H_2O)_2].2H_2O$	222-224	Dark green [90]	7.74 (7.72)	50.68 (50.64)	3.72 (3.71)	7.39 (7.34)	8.46 (8.45)	9.35 (9.34)	10.20
(2)$[Cu(L)_2(H_2O)_2]$	212-214	Dark brown [84]	8.33 (8.34)	50.36 (50.32)	3.70 (3.56)	7.34 (7.33)	8.40 (8.38)	9.29 (9.22)	10.12
(3)$[Cd(L)_2(H_2O)_2].H_2O$	245-247	Orange [88]	14.16 (14.11)	48.40 (48.35)	3.30 (3.27)	7.06 (7.00)	8.08 (8.03)	8.93 (8.90)	7.07

$^a\Lambda_m$: molar conductance (ohm^{-1} cm^2 mol^{-1})

The electronic spectral data of HL ligand in ethanol and hexane are presented in Table 3. The wavelengths of the absorption bands appeared in the UV region in both solvents are practically identical. From the relatively higher intensity the band at 45,045–33,898 nm are assigned to π→π* transitions of the enol–imine tautomer of the Schiff base ligand. The observed small hypsochromic shift (~ 2 nm) of the 30,303 nm band in more polar solvents is typical to n→π* transitions of C=N group [18]. The maximum at 24,096 nm detected in the EtOH solutions of HL ligand, is assigned to n→π* transitions in dipolar zwitterionic or keto–imine tautomeric structures, respectively [19].

^{1}H NMR spectra of HL ligands in DMSO-d6, without and with D_2O are shown in Figure 2. The assignments of the ^{1}H NMR spectral characteristics of HL ligand are presented in Table 4. The phenolic OH group shows that proton signal was assigned at 14.00 ppm. This peak is due to hydrogen bonded phenolic protons and the integration is generally less than 2.0 due to this intramolecular hydrogen bonding. Signal for the methine proton of the characteristic azomethine group for Schiff base, –N=CH– were observed at 8.88 ppm. In the region of 7.29–6.88 ppm chemical shifts were assigned for hydrogen of the aromatic ring. The ^{13}C NMR spectrum of the ligand (Figure 3) is concordant with different types of magnetically non-equivalent carbons. The peak at 173.38 ppm is due to azomethine carbon (–CH=N–).

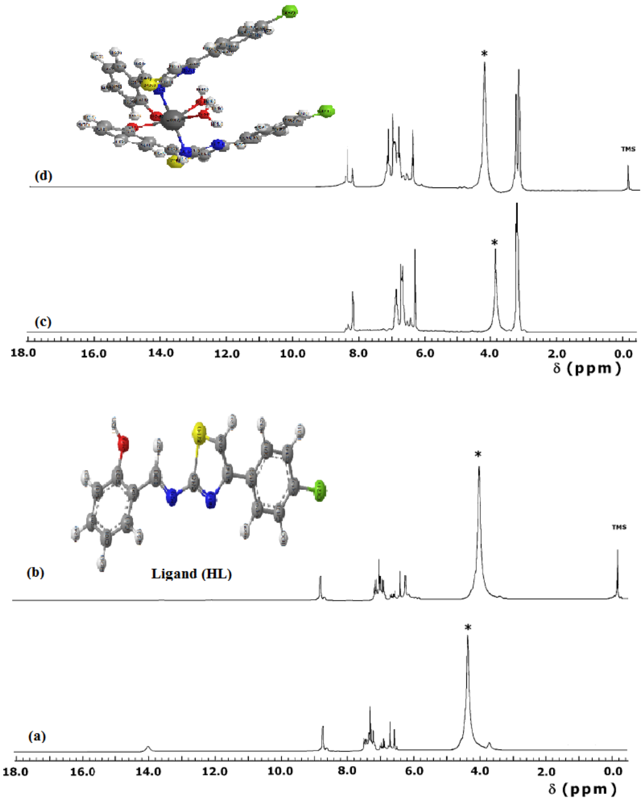

Figure 2. ^{1}H-NMR spectra (d, ppm) in DMSO-d_6 solvent of the (a) Schiff base, HL, ligand, (b) Schiff base, HL, ligand after the addition of D_2O, (c) Schiff base complex, $[Cd(L)_2(H_2O)_2]H_2O$, and (d) Schiff base complex, $[Cd(L)_2(H_2O)_2]H_2O$, after the addition of the D_2O; (*) suppressed solvent.

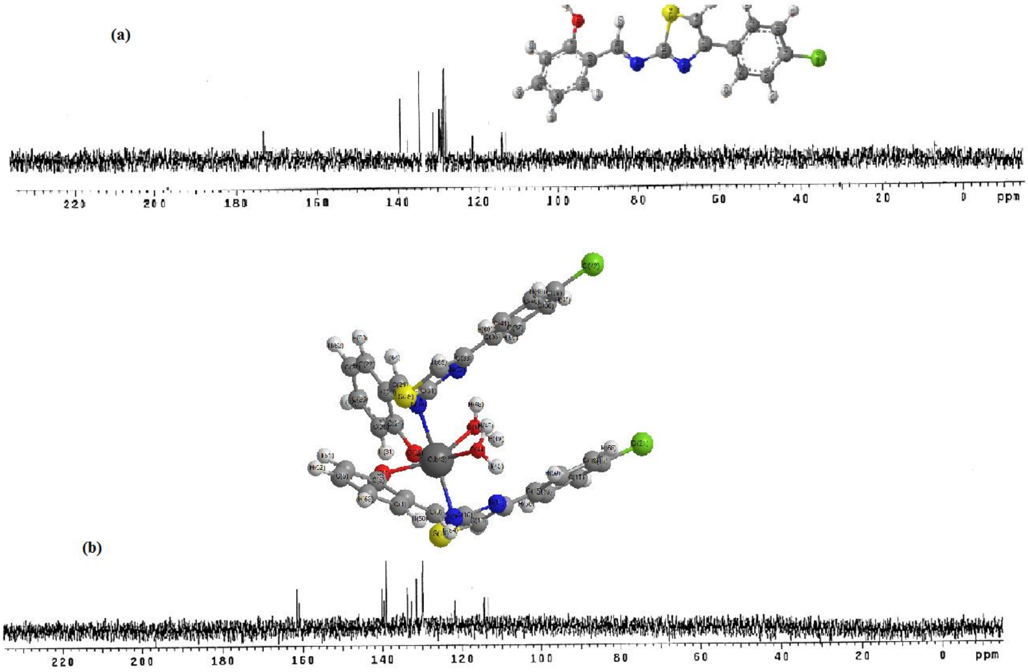

Figure 3. ^{13}C-NMR spectra (d, ppm) in DMSO-d_6 solvent of the (a) Schiff base, HL, ligand and (b) Schiff base complex, $[Cd(L)_2(H_2O)_2]H_2O$.

The electron impact mass spectrum of the free ligand, confirms the proposed formula by showing a peak at 314 u corresponding to the ligand moiety [($C_{16}H_{11}ClN_2OS$) atomic mass 314.79u]. The series of peaks in the range, i.e. 66, 85, 94, 108, 134, 150 and 165 u, etc., may be assigned to various fragments and their intensity gives an idea of stability of fragments.

Quantum chemical calculations using PM3 method are used to investigate the geometry structure of the Schiff base ligand HL. The optimization of bond lengths and bond angles (Supplimentary Table S1) produces a stable structure with a minimum energy.

The molecular orbital calculations show that the phenyl moiety is out of plane with respect to both thiazole and OH–phenyl rings. The bond lengths of C2–C8, C8–N9, and N9–C10 bonds are equal to 1.3370, 1.2600and 1.2632°A, respectively, and the double bond character of C8–N9 bond is a good evidence for Schiff base formation. The C3–O7 bond length 1.3550°A donates some double bond character of this bond. The partial double bond character of the C–O bond confirms the proposed keto–enol tautomerism represented in Figure 4 since the bond would have resonance character between a double bond and a single one. The calculations reveal the formation of strong hydrogen bond, N9–H27, as assumed before with bond length equal to 1.4543°A, and confirmed by the presence of the negative charge on N9 equal to 0.22387 e.

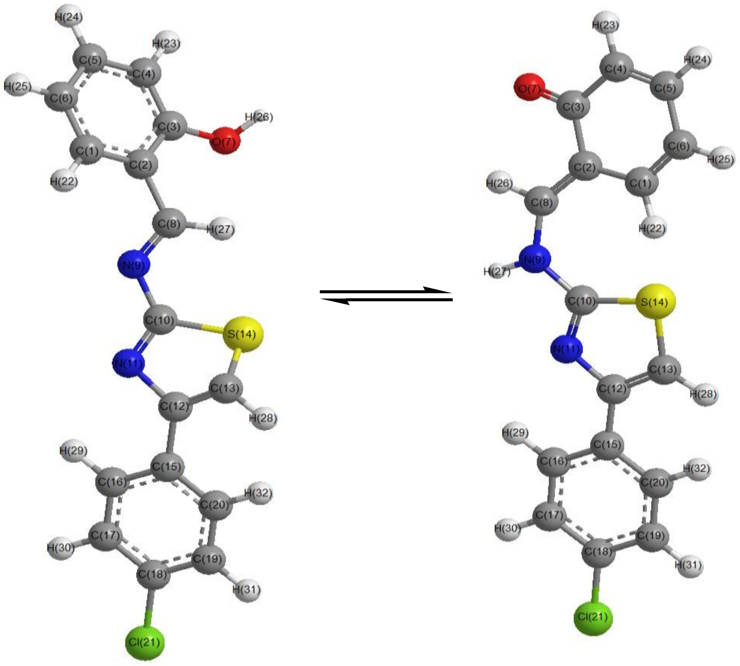

Figure 4. PM3 optimized structure of HL showing atomic numeration.

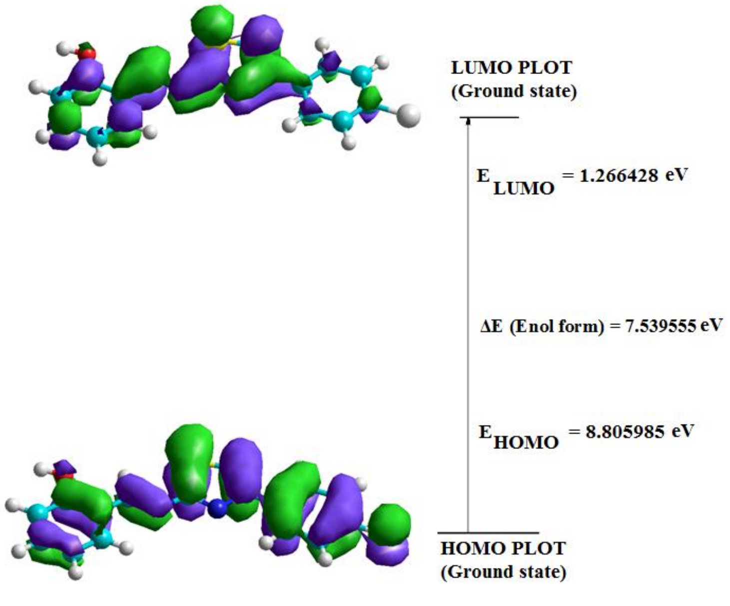

Figure 5. The atomic orbital compositions of the frontier molecular orbital for HL ligand in enol-form.

Ferraz et al. [20] reported the bond length of C–S = 1.749 ˚A for thiosemicarbazones metal complexes. In our present study the C–S bond length is 1.7154 A˚, found to be good agreement with 1.7161 A˚ for our title molecule.

On the other hand, while the energy of the HOMO is directly related to the ionization potential, LUMO energy is directly related to the electron affinity. Energy difference between HOMO and LUMO orbital is called as energy gap that is an important stability for structures [21]. In addition, 3D plots of highest occupied molecular orbitals (HOMOs) and lowest unoccupied molecular orbitals (LUMOs) are shown in Fig. 5, 6. According to PM3 calculation, The HOMO and LUMO (Table 5, Figure 5,6) energies of the enol-form are found to be 8.805983 and 1.266428 eV (ΔE = 7.539555 eV), respectively, while that for the keto-form are 8.558686 and 1.457075 eV (ΔE = 7.101611 eV), respectively.

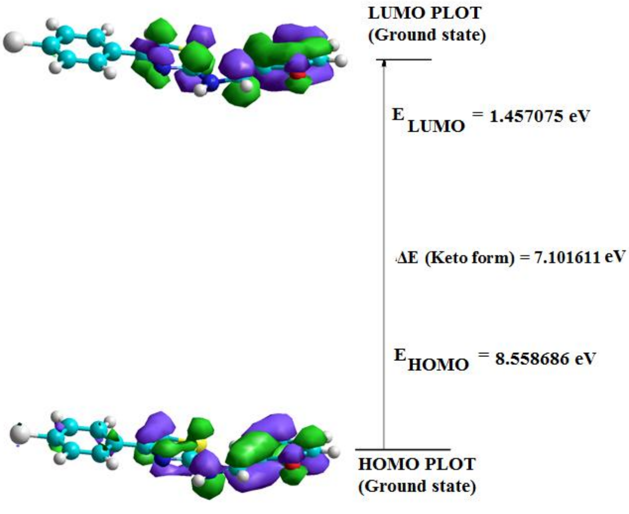

Figure 6. The atomic orbital compositions of the frontier molecular orbital for HL ligand in keto-form.

4.2. Complexes

4.2.1. Molar conductance measurements

The results given in Table 1 show that the Ni(II), Cu(II) and Cd(II) complexes have a molar conductivity values in the range 7.07–10.20 Ω^{-1} mol^{-1} cm^2, which indicates the non–ionic nature of these complexes and they are considered as non–electrolyte [22]. This implies the coordination of the anions to the metal ion centers.

4.2.2. IR spectra

The prominent infrared spectral data of Schiff base and its metal complexes (Figure 1) are presented in Table 2. IR spectra of the ligand shows band at 3445 cm^{-1}, which can be attributed to phenolic OH group. This band disappears in all complexes, which can be attributed to involvement of phenolic OH in coordination. The involvement of deprotonated phenolic OH group in complexes is confirmed by the shift of ν(C–O) stretching band observed at 1212 cm^{-1} in the free ligand to the lower frequency to the extend of 10–15 cm^{-1} [23, 24]. The azomethine vibration of the ligand at 1641 cm^{-1} was shifted to lower frequency after complexation, which is 1615, 1614 and 1612 cm^{-1} for Ni(II), Cu(II) and Cd(II) complexes, respectively. The unchanged bands after complexation at 1578 and 743

cm^{-1} in the free ligand suggests non-involvement of the coordination which was assigned as ν(C=N) thiazole ring and ν(C–S–C), respectively [25]. A weak band around 292 cm^{-1} in the complexes is absent in the ligand spectrum assigned to ν(M–N) vibration. Another weak band appeared in the spectra of the complexes at about 340–3429 cm^{-1} attributed to ν(M–O) vibration. The bands in the range 788–836 cm^{-1} and 624–633 cm^{-1} appeared in the spectra of these complexes which may be assigned to ρr(H_2O) and ρw(H_2O) [26-29].

From these observations, it was suggested that the azomethine nitrogen and hydroxyl oxygen are involved in the complexation reaction as donor atoms.

Table 2. Characteristic IR bands of the ligand and its metal complexes

Assignments	Ligand	$[Ni(L)_2(H_2O)_2].2H_2O$	$[Cu(L)_2(H_2O)_2]^{-2}$	$[Cd(L)_2(H_2O)_2].H_2O$
$\nu(OH)$	3445 br	–	–	–
ν(C–O)	1212m	1102m	1200m	1197m
$\nu(C{=}N)_{azomethine}$	1641m	1615m	1614m	1612m
$\nu(C{=}N)_{thiazole}$	1578m	1579m	1578m	1577m
$\nu(C–H)_{aromatic}$	3034m	3034m	3032m	3032m
ν(C–S–C)	743s	741s	742s	743s
$\rho r(H_2O)$	-	788v.s	836s	827s
$\rho w(H_2O)$	-	633s	624s	630s
δ(O–M–O)	-	193w	192v.w	193w
δ(O–M–N)	-	233w	232w	233w
ν(M–N)	-	292w	290w	294w
ν(M–O)	-	341w	340w	342w

br = broad, s = strong, m = medium, w = weak, v.s = very strong , v.w = very weak.

4.3. NMR spectra

4.3.1. ^{1}H NMR spectral analysis

In the ^{1}H NMR spectra, the integral intensities of each signal were found to agree with the number of different types of protons present in the complex. A signal appeared in the ligand ^{1}H NMR spectrum at δ=8.88 is due to CH=N protons. However, in the spectra of cadmium complex the signal was moved up–field at δ=8.27 suggests the coordination of imino nitrogen to cadmium ion [22, 23]. The hydroxyl proton of the ligand was observed at 14.00 ppm. However, this was not present in the complex spectrum due to the involvement of hydroxyl oxygen in chelation through deprotonation. On the other hand, the signal observed at 3.32 ppm with an integration corresponding to five protons in case of Cd(II) complex is assigned to three water molecules.

4.3.2. ^{13}C NMR spectral analysis

In the ^{13}C spectra of Cd(II) complex a up-field shift of CH=N group was observed in at 161.43 ppm. It signifies that the ligand coordinates through the nitrogen atom of CH=N [30,31]. However, the enolic carbon peak shifted to 139.93 δ suggesting that coordination of C–O group to the metals by deprotonation. The ^{1}H and ^{13}C NMR spectrum of $[Cd(L)_2(H_2O)_2]H_2O$ mononuclear complex is given in Figs. 2 and 3.

4.4. Magnetic properties, electronic spectra, ESR measurements

The electronic absorption spectra of the metal complexes under investigation were recorded within the range 12,500–25,000 cm^{-1} applying the nujol mull technique and in DMF solution.

The Ni(II) complex shows a magnetic moment 2.92 B.M. recorded at room temperature, corresponding to two unpaired electrons. The electronic spectra of Ni(II) complex (**1**) exhibit two bands with no obvious difference on going from nujol mull to DMF solution at (13,845, 15,413), cm^{-1}. These bands are assigned to $^{3}A_{2}g\rightarrow{}^{3}T_{1}g$ (F) and $^{3}A_{2}g \rightarrow{}^{3}T_{1}g$ (P) transitions which may indicate octahedral geometry around Ni(II) ions [26, 32, 33].

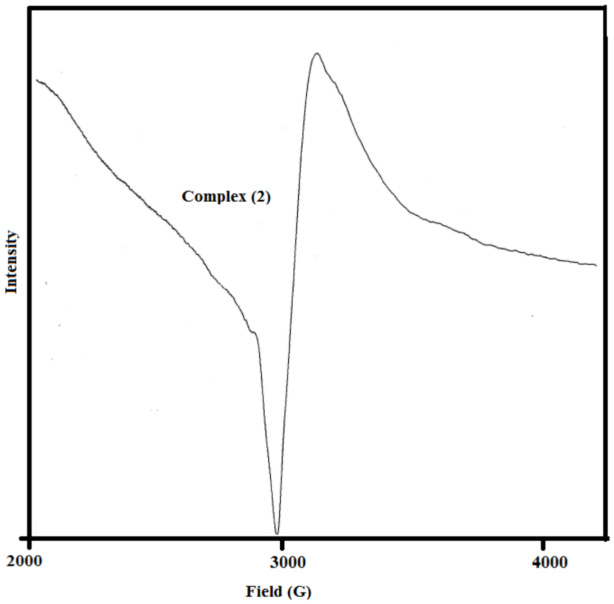

Figure 7. X-Band esr spectra in the solid state at 25 °C of the $[Cu(L)_2(H_2O)_2]$ complex.

Copper(II) complex show room temperature magnetic moment 1.85 B.M., corresponding to one unpaired electron. The positions of the bands of Cu(II) complexes in nujol mull spectra exhibit some shifts to lower wavelength in DMF solution to 16,222 and 15,835 cm^{-1}, respectively, indicating the facile formation of six coordinate species in DMF and solid state which are a coordinating.

In case of Cu(II) complex (**2**) the electronic spectra in DMF solution exhibit bands at (13,753, 16,128) cm^{-1} and in nujol mull at (13,928, 16,479) cm^{-1}, which can be assigned to $^{2}B_{1}g\rightarrow{}^{2}Eg$ and $^{2}B_{1}g\rightarrow{}^{2}B_{2}g$ transitions within octahedral structures [26, 34,35]. The ESR spectrum of Cu(II) complex

(**2**) gives three anisotropic signals ($g\perp = gx = 2.4188$, $g_{\|} = gz = 2.7354$ and $g_y = 2.6208$) and $g_{\text{eff}} = 2.6005$ which confirm the octahedral geometry around the Cu(II) ion. ESR spectrum of Cu complex is given in Figure 7.

The Cd(II) complex is found to be diamagnetic as expected for d^{10} configuration. The electronic spectrum of the Cd(II) complex shows an absorption band at 23,667 cm^{-1} attributed to the LMCT transition, which is compatible with this complex having an octahedral structure [36,37].

4.5. Mass spectra

The mass spectra of complexes showed peaks attributed to the molecular ions m/z at 653 M+, 727 M+ and 794 M+ for nickel, copper and cadmium(II)complex complexes, respectively.

4.6. Electrochemistry

Cyclic voltammograms of $[Ni(L)_2(H_2O)_2].2H_2O$, $[Cu(L)_2(H_2O)_2]$ and $[Cd(L)_2(H_2O)_2]H_2O$ were recorded in degassed DMF with 0.1m tetrabutylammonium hexafluorophosphate (TBAP) as supporting electrolyte. The electrochemical data obtained at a glassy carbon electrode in DMF solution are recorded. The cyclic voltammogram of nickel complex shows well defined redox process corresponding to the formation of the quasi–reversible Ni(II)/Ni(I) couple. The anodic peak at E_{pa}= 0.5 V and the associated cathodic peak at E_{pc}=1.5 V corresponds to Ni(II)/Ni(I) couple [38].

The copper complex is redox active and show a cyclic voltammogram response in the potential range 0.7–1.7V [18–20] assigned to the Cu(II)/Cu(I) couple. The nonequivalent current intensity of cathodic and anodic peaks (ic/ia=0.7 V) indicates a quasi–reversible behavior [39]. It has been shown that the formal redox potential of Cu(II)/Cu(I) couple is dependent on factors such as coordination number, hard/soft nature of the ligands and bulkiness of the ligands [40].

The cyclic voltammogram of Cd(II) complex in DMF solution in the absence of molecular oxygen at room temperature in 0.1 to –1.0 V potential range at scan rate 50 mVs^{-1} indicating quasi-reversible one–electron process. A noteworthy feature has been observed in the cyclic voltammogram of Cd(II) complex. During the forward scan it shows two cathodic reduction peaks, one at +0.43 V and another at –0.67 V which are attributed to reduction of Cd(II) → Cd(I) and Cd(I) → Cd(0) respectively. During the reverse scan it shows two anodic oxidation peaks, one at –0.28 V and another at +0.65V which are attributed to oxidation of Cd(0)→ Cd(I) and Cd(I)→ Cd(II) respectively [23].

4.7. X-ray powder diffraction analysis

All complexes $[Ni(L)_2(H_2O)_2].2H_2O$, $[Cu(L)_2(H_2O)_2]$ and $[Cd(L)_2(H_2O)_2]H_2O$ were found to be crystalline and their X-ray powder diffractograms were collected. The lattice parameters and Miller indices were computed. The indexing and calculation of unit cell parameters are performed with the help of Powder–X Software. The calculated and observed 2θ value (Figure 8), the relative intensity, interplanar distance along with Miller's indices for corresponding angles are tabulated for the complexes. On the basis of X–ray powder patterns and unit cell refinements, it is found that all the complexes adopt triclinic crystal system with p–type of lattice space group. The lattice constants calculated, $[Ni(L)_2(H_2O)_2].2H_2O$, $[Cu(L)_2(H_2O)_2]$ and $[Cd(L)_2(H_2O)_2]H_2O$ complexes are depicted in Table 3.

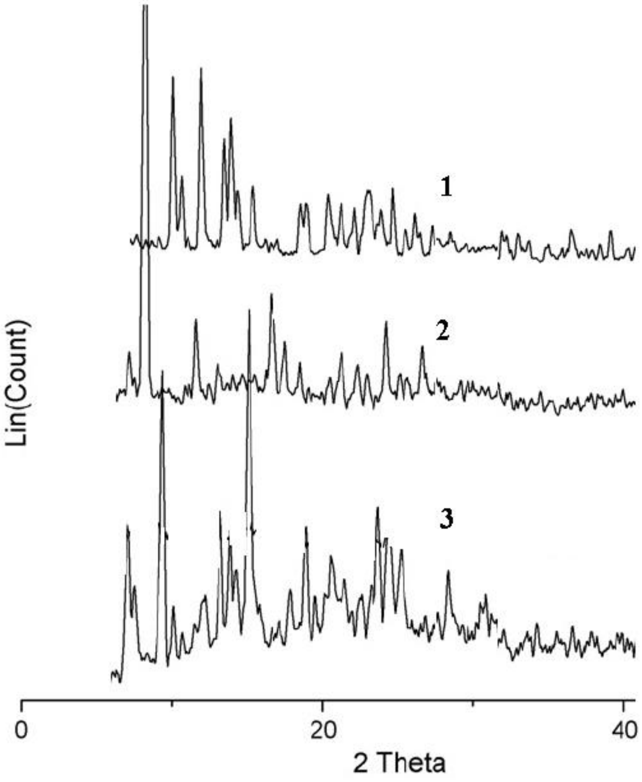

Figure 8. X–ray diffraction patterns of (1) Ni(II), (2) Cu(II) and (3) Cd(II) complexes.

Table 3. Crystallographic data for the Schiff base complexes$[Ni(L)_2(H_2O)_2].2H_2O$, $[Cu(L)_2(H_2O)_2]$ and $[Cd(L)_2(H_2O)_2].H_2O$.

Data	$[Ni(L)_2(H_2O)_2].2H_2O$	$[Cu(L)_2(H_2O)_2]$	$[Cd(L)_2(H_2O)_2].H_2O$
Empirical formula	$C_{32}H_{28}Cl_2N_4NiO_6S_2$	$C_{32}H_{24}Cl_2CuN_4O_4S_2$	$C_{32}H_{26}Cl_2N_4O_5S_2Cd$
Formula weight (g/mol)	653.43	727.17	794.02
Crystal system	Triclinic	Triclinic	Triclinic
Space group	P−1	P−1	P−1
Unit cell dimensions(Å,°)			
a(Å)	8.8355	86588.	8.2633
b(Å)	10.5872	10.1543	10.8952
c(°)	14.5575	14.7789	14.7459
α(°)	105.234	71.812	98.5784
β(°)	91.278	73.020	88.5986
γ(°)	114.209	89.8	111.4582
Volume (Å)	132.75	139.30	129.50
(Calc.) density (g/cm^{-3})	4.9222	5.2201	6.1314
Temperature (K)	293	293	293

4.8. Thermal analyses

Thermal behavior of the complexes has been studied using TGA, and DTA analysis. Based on the thermograms, decomposition stages, temperature ranges, decomposition product as well as weight loss percentages of the complexes were calculated. The complexes $[Ni(L)_2(H_2O)_2].2H_2O$ and $[Cd(L)_2(H_2O)_2].H_2O$ undergo decomposition mainly in three stages. In the first stage a peak corresponding to the loss of the water molecule in the temperature range of 60–115 °C was observed. The expulsion of water molecules in this range indicates that they are lattice held. It is further evidenced by an endothermic peak in the above temperature range in DTA curve, indicating that the water molecules are of lattice type. The second stage corresponds to the loss of water molecules in the temperature range of 180–210 °C corresponding to the loss of coordinated water molecules. The presence of endothermic peak at 190–210 °C in DTA curve of the complex also further confirms the presence of coordinated water. The third stage corresponds to the loss of organic moiety. The final decomposition of the complexes above 650 °C corresponds to metal oxide.

The thermogram of $[Cu(L)_2(H_2O)_2]$ complex shows only two stages of decomposition. The first stage corresponds to coordination of water molecules at 175 °C and second stage being the loss of organic moiety. The presence of water molecules is further evidenced by DTA curves. The expulsion of water molecules and the percentage of loss of weight in the above temperature range indicate that water molecules are not hydrated [41]. The analysis of the thermogram by the way of identifying the final products offers further support to the composition of the complexes proposed on the basis of elemental and spectral analysis.

4.8.1. Molecular modeling of complexes

HL and its complexes are shown in (Figures 1, 9, 10, 11). Analysis of the data in Tables (1S–4S) (Supplementary Materials) calculated for the bond lengths and angles for the bond, one can conclude the following remarks:

1. The metal–oxygen (aquo) bond lengths (1.8547, 1.9126 Å) in $[Ni(L)_2(H_2O)_2].2H_2O$, (2.0804, 2.0554Å) in $[Cu(L)_2(H_2O)_2]$ and (2.1497, 2.1495Å) in $[Cd(L)_2(H_2O)_2].H_2O$ are quite longer than the metal–oxygen (Schiff base) bond lengths (1.8241, 1.8471 Å), (1.9676, 1.8486Å) and (2.0887, 2.0799Å) validating the labile nature of metal-aquo linkages. The geometries of the complexes $[Ni(L)_2(H_2O)_2].2H_2O$, $[Cu(L)_2(H_2O)_2]$ and $[Cd(L)_2(H_2O)_2].H_2O$ remains almost unaffected upon substitution of axial aquo groups.

2. The bond angles of the Schiff base moiety are altered somewhat upon coordination; the largest change affects C2–C3–O7 angle which are change from 119.9999° on ligand to 125.8204° on complexes as a consequence of bonding in case of $[Cu(L)_2(H_2O)_2]$complex while in case of $[Cd(L)_2(H_2O)_2].H_2O$ complex the largest change affects C2–C8–N9 from 120.0000° to 146.5902° finally in case of $[Ni(L)_2(H_2O)_2].2H_2O$ complex the largest change affects C(8)–N(9)–C(10) from 120.0000° to 135.7833°.

3. The energy optimized structures of the complexes (Figs. 3 and 4) and the geometrical parameters (Table 4) suggest a distorted octahedral structure predicting sp^3d^2 hybridization.

4. The HOMO and LUMO energies of the complex $[Cu(L)_2(H_2O)_2]$ are found to be 4.45 and 1.26 eV (ΔE = 3.19 eV), respectively, while that for the complex $[Ni(L)_2(H_2O)_2].2H_2O$ are 6.46 and 1.35 eV (ΔE = 5.11 eV), respectively, finally in case of $[Cd(L)_2(H_2O)_2].H_2O$ complex are 8.38 and 1.34 eV (ΔE = 7.04 eV), respectively (Table 4).

Table 4. Some energetic properties of ligand **( )** and its complexes calculated by PM3 method

	Total energy kcal/mol	Binding energy kcal/mol	Electronic energy kcal/mol	Core-Core Interaction	Heat of formation kcal/mol	Dipole moment	HOMO	LUMO
Ligand Enol-Form	-73423.0434140	-3624.2685920	-466849.3915917	393426.3481777	64.0424080	3.777	8.805983	1.266428
Ligand Keto-Form	-73408.7936445	-3610.0188225	-474836.8243678	401428.0307234	78.2921775	3.020	8.558686	1.457075
Cu	-188504.1777710	-7750.6761110	-1879079.3625613	1690575.1847903	-70.0321110	2.508	4.452151	1.261556
Ni	-185280.8544645	-7937.7287895	-1891534.0424237	1706253.1879592	-234.9847895	10.799	6.466531	1.347881
Cd	-161605.4508788	-7542.1971548	-1529450.4565574	1367845.0056786	–84.4668452	8.234	8.38317	1.347881

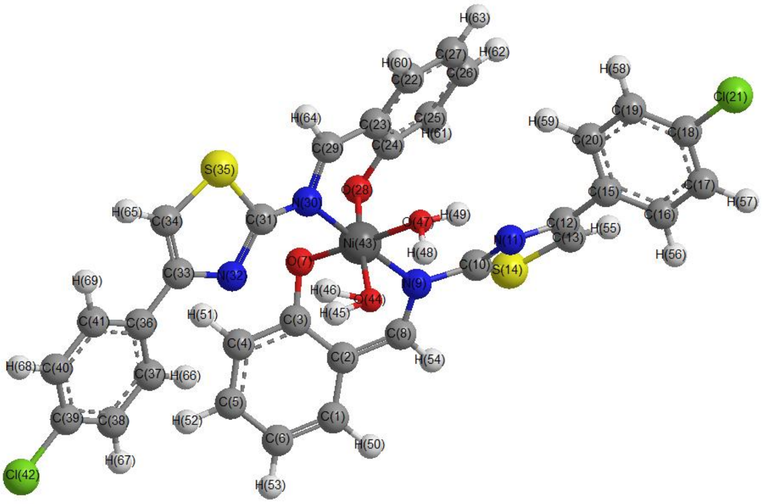

Figure 9. Optimized structure of $[Ni(L)_2(H_2O)_2]2H_2O$ complex at PM3.

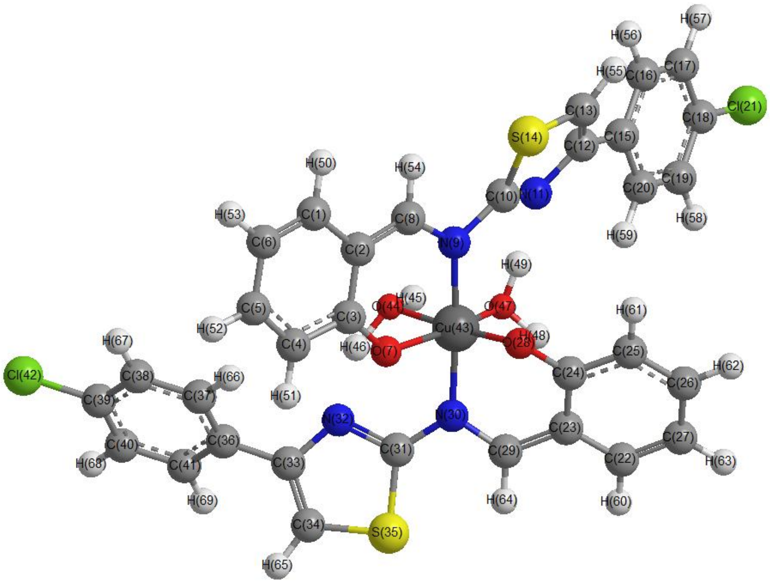

Figure 10. Optimized structure of $[Cu(L)_2(H_2O)_2]$ complex at PM3.

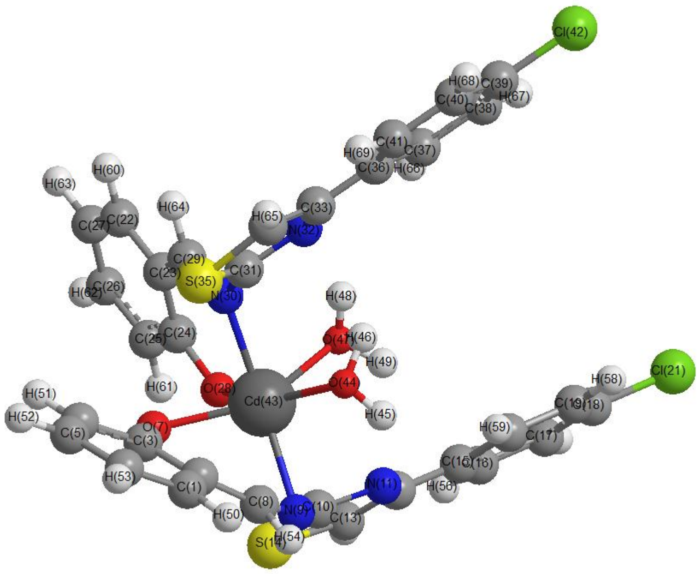

Figure 11. Optimized structure of $[Cd\ (L)_2(H_2O)_2]H_2O$ complex at PM3.

4.9. Antimicrobial activity

The minimum inhibitory concentration (MIC) values of the compounds are given in Table 5. From the in vitro antimicrobial screening results (Table 5), it is observed that the ligand is moderately active against bacteria, *E. coli*, *P. phaseolicola* and fungi, *A. niger*.

Table 5. Minimum inhibitory concentration (MIC) results of the synthesized compounds ((g/mL).

Ligand/complexes (1000µg/ml)	Zone of inhibition (mm)					
	Gram–positive bacteria		Gram–negative bacteria		Fungal	
	S. aureus	*S. pyogenes*	*E. coli*	*P. phaseolicola*	*A. niger*	*A. flavus*
HL	>100	80	>100	85	>100	80
$[Ni(L)_2(H_2O)_2]2H_2O$	>100	97	>100	92	>100	88
$[Cu(L)_2(H_2O)_2]$	27	18	14	24	34	45
$[Cd(L)_2(H_2O)_2]H_2O$	10	09	08	21	05	04
Streptomycin[a]	11	9	05	05	–	–
Ampicillin[a]	12	10	07	06	–	–
Rifampicin[a]	48	50	47	44	–	–
Nystatin[a]	–	–	–	–	10	08

[a] Standard.

The complexes have shown higher activity in comparison with the ligand against both bacteria and fungi used. The activity of the ligand has enhanced on complexation, which can be explained on the basis of Overtone's concept and Tweedy's chelation theory [42]. Among the complexes, $[Cd(L)_2(H_2O)_2].H_2O$ complex has the highest potential against all the microorganisms, which is even more than the standard drugs used. $[Ni(L)_2(H_2O)_2].2H_2O$ and $[Cu(L)_2(H_2O)_2]$ complexes showed lower activity against *E. coli* and *C. albicans* as compared with the free ligand. As seen in Table 5, it can be concluded that the cadium complex have higher antimicrobial activity than the nickel(II) and copper(II) complexes. This may be due to the presence of cadmium metal in the second row transition elements and the cadmium(II) ion is found to be diamagnetic as expected for d^{10} configuration, while the nickel and copper metals are found in the first row transition elements in periodic table, and all nickel(II) and copper(II) ions are paramagnetic because The magnetic measurements show the presence of two and one unpaired electrons in Ni(II) and Cu(II) complexes, respectively [43,44].

ACKNOWLEDGEMENT
This project was supported by King Saud University, Deanship of Scientific Research, the Research Center, College of Science, King Saud University.
.

References

1. Y. Shibuya, K. Nabari, M. Kondo, S. Yasue, K. Maedo, F. Uchida, H. Kawaguchi, *J. Chem. Lett*. 37(2008)78.
2. M. Bera, U. Mukhopadhyay, D. Ray, *Inorg. Chem. Acta* 358 (2005) 437.
3. L. A. Saghatforoush, F. Chalabian, A. Aminkhani, G. Karimnezhad, S. Ershad, *Eur. J. Med. Chem*. 44 (2009) 4490.
4. J.Z. Wu, L. Yuan, J. Inorg. Biochem. 98 (2004) 41.
5. K.P. Balasubramanian, K. Parameswari, V. Chinnusamy, R. Prabhakaran, K. Natarajan, *Spectrochim. Acta* A 65 (2006) 678.
6. S. Bondock, W. Fadaly, M.A. Metwally, *Eur. J. Med. Chem*. 45 (2010) 3692.
7. J. Vanco, J. Marek, Z. Travnicek, E. Racanska, J. Muselik, O. Svajlenova, *J. Inorg. Iochem*. 102 (2008) 595.
8. V.C. Silveira, J.S. Luz, C.C. Oliveira, I. Graziani, M.R. Ciriolo, A.M.C. Ferreira, *J. Inorg. Biochem.* 102 (2008) 1090.
9. A.T. Chaviara, P.J. Cox, K.H. Repana, R.M. Papi, K.T. Papazisis, D. Zambouli, A.H. Kortsaris, D.A. Kyriakidis, C.A. Bolos, *J. Inorg. Biochem*. 98 (2004) 1271.
10. S.B. Desai, P.B. Desai, K.R. Desai, *Heterocycl. Commun*. 7 (2001) 83.
11. P. Pathak, V.S. Jolly, K.P. Sharma, *Orient. J. Chem*. 16 (2000) 161.
12. S. Allah, A.M. Abid, Phosphorus, *Sulfur Silicon Relat. Elem*. 170 (2001) 75.
13. T.P. Yoon, E.N. Jacobsen, *Science* 299 (2003) 1691.
14. T. Yamada, T. Ikeno, Y. Ohtsuka, S. Kezuka, M. Sato, I. Iwakura, *Sci. Technol. Adv. Mater*. 7 (2006) 184.
15. Y.P. Cai, C.Y. Su, A.W. Xu, B.S. Kang, H.Q. Liu, S. Jie, *Polyhedron* 20 (2001) 657.
16. HyperChem Version 8.03 Hypercube, Inc.
17. N.L. Allinger, *J. Am. Chem. Soc*. 99 (1977) 8127.
18. V.T. Kasumov, A.I. Öztürk, F. Köksal, *Polyhedron* 26 (2007) 3129–3135.
19. P.W. Alexander, R.J. Sleet, *Aust. J. Chem*. 23 (1970) 1183–1190.
20. K.O. Ferraz, S.M.S.V. Wardell, J.L. Wardell, S.R.W. Louro, H. Beraldo, *Spectrochim. Acta* 73A (2009) 140.
21. K. Fukui, Theory of Orientation and Stereoselection, Springer-Verlag, Berlin, 1975, see also: Fukui, K. *Science* 218 (1987) 747.
22. W.J. Geary, *Coord. Chem. Rev*. 7 (1971) 81–122.
23. V. Selvarani, B. Annaraj, M.A. Neelakantan, S. Sundaramoorthy, D. Velmurugan, *Spectrochim. Acta* A 91 (2012) 329– 337.

24. M.M. Omar, G.G. Mohamed, *Spectrochim. Acta, Part* A 61 (2005) 929.
25. R. Castro, J.A. Garcia-Vazquez, J. Romero, A. Sousa, *Polyhedron* 12 (1993) 47.
26. A. M.A. Alaghaz, R.A. Ammar, *Eur. J. Med. Chem*. 45 (2010) 1314–1322.
27. P.J. Lucchesi, W.A. Glasson, *J. Am. Chem. Soc*. 78 (1956) 1347.
28. T.M. El-Gogary, A.M.A. Alaghaz, R.A.A. Ammar, *J. Mol. Str*. 1011 (2012) 50–58.
29. A.M.A. Alaghaz, A.G. Al-Sehemi, T.M. EL-Gogary, *Spectrochim. Acta* A 95 (2012) 414–422.
30. K. Shanker, P.M. Reddy, R. Rohini, Y.P. Ho, V. Ravinder, *J. Coord. Chem*. 62 (2009) 3040–3049.
31. K. Shanker, R. Rohini, K. Shravankumar, P.M. Reddy, Y.P. Ho, V. Ravinder, *J. Ind. Chem. Soc*. 86 (2009) 153–161.
32. F.A. Cotton, G. Wilkinson, Advanced Inorganic Chemistry, Interscience Publishers, London, 1974.
33. S.J. Swamy, S. Pola, *Spectrochim. Acta* Part A 70 (2008) 929–933.
34. S. Sreedarana, K.S. Bharathia, A.K. Rahimana, R. Suresha, R. Jegadeeshb, N. Raamanb, V. Narayanana, *Spectrochim. Acta* Part A 74 (2009) 849–854.
35. K. Karaoglu, T. Baran, K. Serbest, M. Er, I. Degirmencioglu, *J. Mol. Struct*. 922 (2009) 39–45.
36. Z.H. Chohan, H.H. Parvez, *Synth. React. Inorg. Met.-Org. Chem.* 23 (1993) 1061
37. M. Sekerci, E. Tas, *Heteroatom Chem.* 11 (2000) 254.
38. A.J. Bard and L.R. Izatt, Electrochemical method: Fundamentals and Applications: 2nd Ed., Wiley: New York, 2001.
39. A.A. Khumhar, S.B. Rendye, D.X. West, A.E. Libbert, *Transition Met Chem*., 16 (1991) 276.
40. A.S. Kumbhar, S.B. Padhye, D.X. West, A.E. Liberta, *Transition Met Chem*., 17 (1992) 247.
41. P.M. Reddy, A.V.S.S. Prasad, V. Ravinder, *Transit. Met. Chem*. 32 (2007) 507–513.
42. N.P. Priya, S.V. Arunachalam, N. Sathya, V. Chinnusamy, C. Jayabalakrishnan, *Trans. Met. Chem*. 34 (2009) 437–442.
43. C.J. Ballhausen, An Introduction to Ligand Field Theory, third ed. McGraw Hill, New York, 1962.
44. A.A. Khandar, B. Shaaban, F. Belaj, A. Bakhtiari, *Polyhedron* 25 (2006) 1893–1900.